ECS Journal of Solid State
Science and Technology

Temperature-Pressure Phase Diagram and Possible Pressure-Driven New Electronic Phase in the Polar Metal $LiOsO_3$

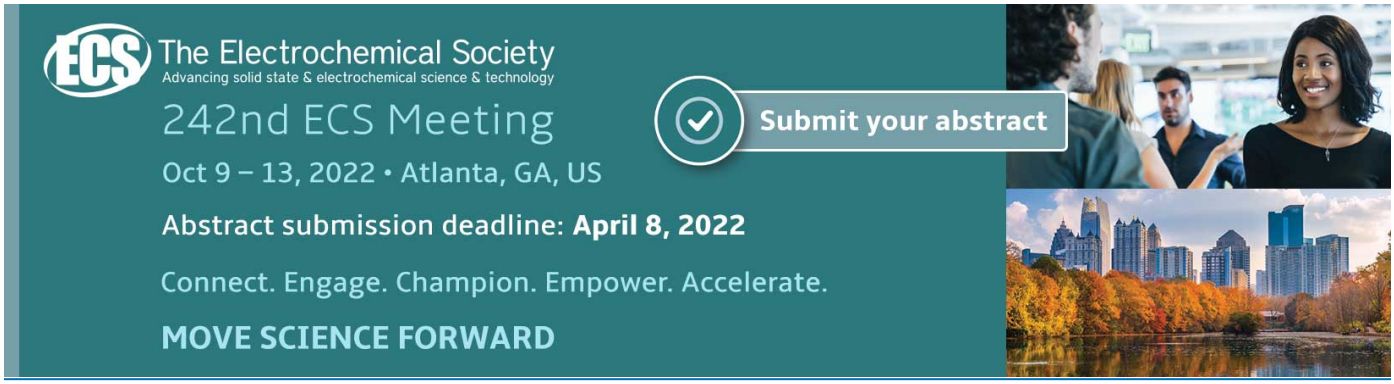

ECS Journal of Solid State Science and Technology, 2022 **11** 023008
2162-8777/2022/11(2)/023008/4/$40.00 © 2022 The Electrochemical Society ("ECS"). Published on behalf of ECS by IOP Publishing Limited

Temperature-Pressure Phase Diagram and Possible Pressure-Driven New Electronic Phase in the Polar Metal $LiOsO_3$

J.-G. Cheng,[1,2,z] J.-S. Zhou,[3] and Y. Uwatoko[2]

[1]*Beijing National Laboratory for Condensed Matter Physics and Institute of Physics, Chinese Academy of Sciences, Beijing 100190, People's Republic of China*
[2]*Institute for Solid State Physics, University of Tokyo, Kashiwa, Chiba 277-8581, Japan*
[3]*Materials Science and Engineering Program, Mechanical Engineering, University of Texas at Austin, Austin, Texas 78712, United States of America*

$LiOsO_3$ is a strongly correlated metal that undergoes a nonpolar to polar transition at the critical temperature (T_s) of 140 K. Complementary to previous studies of structure, Raman, and resistivity under high pressure (P), here we map out a complete pressure evolution of $T_s(P)$ via high-pressure resistance measurements up to 18.5 GPa by using a low-temperature multianvil apparatus. Our results show that $T_s(P)$ first increases linearly with pressure at a large slope as reported and then levels off gradually at pressures above 10 GPa when approaching room temperature (295 K). Interestingly, we find that the resistance $R(T)$ of $LiOsO_3$ at 18.5 GPa in the polar *R3c* phase exhibits a distinct temperature profile in comparison with those at lower pressures, signaling the possible occurrence of pressure-driven new electronic phase. The critical pressure for this transition is determined to be $P_c \approx 16.8$ (1) GPa based on the pressure-dependent resistance measurement at room temperature.
 [DOI: 10.1149/2162-8777/ac5472]

Manuscript submitted December 17, 2021; revised manuscript received February 2, 2022. Published February 25, 2022. *This paper is part of the JES/JSS Joint Focus Issue In Honor of John Goodenough: A Centenarian Milestone.*

$LiOsO_3$ synthesized under high pressure is the first experimental realization of "ferroelectric metal."[1] At ambient conditions, it crystallizes in a centrosymmetric structure with space group $R\bar{3}c$ (No. 167) and exhibits a metallic conduction. Upon cooling down to $T_s = 140$ K, it undergoes a second-order structural transition to a non-centrosymmetric *R3c* (No. 161) phase associated with the polar displacement of Li^+ ions along the *c*-axis. Such a nonpolar-to-polar transition at T_s is manifested by a pronounced kink-like anomaly in the temperature dependences of resistivity $\rho(T)$ and other physical properties.[1] Since its discovery in 2013, the microscopic mechanisms and regulations of the polar transition in $LiOsO_3$ have been subjected to extensive theoretical[2–10] and experimental[11–19] investigations with an aim to achieve rational design of new functional materials.[20–25]

Since the phase transition at T_s involves unit-cell volume change,[1] the application of hydrostatic pressure or strain[10,26] has been considered as an effective means to regulate the polar phase. In 2018, Aulestia and coworkers[13] investigated the pressure effect on T_s of metallic $LiOsO_3$ by monitoring its resistance anomaly under various pressures up to 6.5 GPa. The pressures were generated by using a piston-cylinder cell and a moissanie anvil cell. They found that $T_s(P)$ increases linearly with pressure at a large slope of $dT_s/dP \approx +17.54$ K GPa^{-1} in the studied pressure range and it reaches about 250 ± 44 K at 6.5 GPa. The transition becomes quite broad at pressures $P > 2$ GPa. An extrapolation from the data of T_s vs P in this study predicts a $T_s = 295$ K at ~9.5 GPa. Such a large positive pressure effect is in strikingly contrast to that of conventional insulating ferroelectrics,[27–29] for which hydrostatic pressure usually suppresses the transition temperature and the ferroelectric polarization. Aided by first-principles calculations,[13] the strong enhancement of $T_s(P)$ in $LiOsO_3$ has been attributed to the fact that pressure stabilizes the polar *R3c* phase having a smaller unit-cell volume than the nonpolar $R\bar{3}c$ phase. Later on, Gao et al.[14] confirmed that the polar phase of $LiOsO_3$ is indeed stabilized at room temperature (295 K) under high pressures; the evidences include the observations of characteristic Raman modes of polar phase and the satisfactory refinements of synchrotron X-ray diffraction (SXRD) patterns with the *R3c* symmetry. It is noteworthy that these two probes indicate different critical pressure (P_c) values; i.e., a complete set of Raman mode for the polar *R3c* phase emerges above $P_c \approx 15.5$ GPa, while the SXRD reveals a lower $P_c \approx 12.6$ GPa. Both values are higher than that predicted from a simple extrapolation in the previous study of resistivity under pressure, implying that the assumption of a linear enhancement of $T_c(P)$ will become invalid at higher pressures. In order to reveal the detailed profile of $T_s(P)$ at $P > 6.5$ GPa, one needs to construct a more comprehensive *T*-*P* phase diagram for $LiOsO_3$.

To this end, we are motived to follow T_s of $LiOsO_3$ to much higher pressures than 6.5 GPa by employing a recently developed two-stage multianvil (MA8) apparatus for low-temperature measurements.[30] In complementary to previous studies, we find that $T_s(P)$ starts to deviate from the linear behavior and exhibits a strong bend over above 10 GPa. Unexpectedly, we discover a new pressure-driven electronic phase transition at $P_c \approx 16.8(1)$ GPa, above which the resistance $R(T)$ of $LiOsO_3$ at 18.5 GPa in the polar phase exhibit a distinct temperature profile in comparison with those at lower pressures.

The $LiOsO_3$ crystals used in the present study were synthesized under high-pressure and high-temperature conditions as described elsewhere.[1,31] Resistance measurements under high pressures were carried out by using a newly developed MA8 apparatus for low-temperature measurements. The schematic drawing in Fig. 1a illustrates the sample configuration for resistance measurement with standard four-terminal method in the MA8 apparatus. Here, the $LiOsO_3$ crystal was suspended by four 20 μm-diameter gold wires in the Teflon capsule filled with Daphne 7373 as the pressure transmitting medium (PTM). Such a multianvil compression geometry together with the adoption of liquid PTM can ensure a relatively good pressure homogeneity. The delicate gold wires are protected by 10 μm-thick gold foils and are introduced to the outside surface of the octahedral gasket to connect directly with the tungsten carbide (WC) anvils. The octahedral gasket with integrated fins was casted in a self-designed mold by using the Ceramacast 584-OF potting compound from Aremco Products, Inc. Figure 1b shows a photo of half octahedron with sample installed in the Teflon capsule. Similar as the standard sample assembly for the MA8 apparatus, the octahedron was arranged in the center of eight WC cubes with truncated corner of 3 mm, and the cluster of WC cubes are held together with six pieces of 0.5 mm-thick Fiber Reinforced Polymer (FRP) pads, which also serve as the insulation to the first stage, Figs. 1c–1d. The electrical contacts were further led out by inserting Cu wires in between the FRP pads and the WC anvils that contact directly with the gold wires/foils on the octahedron's surface.

[z]E-mail: jgcheng@iphy.ac.cn

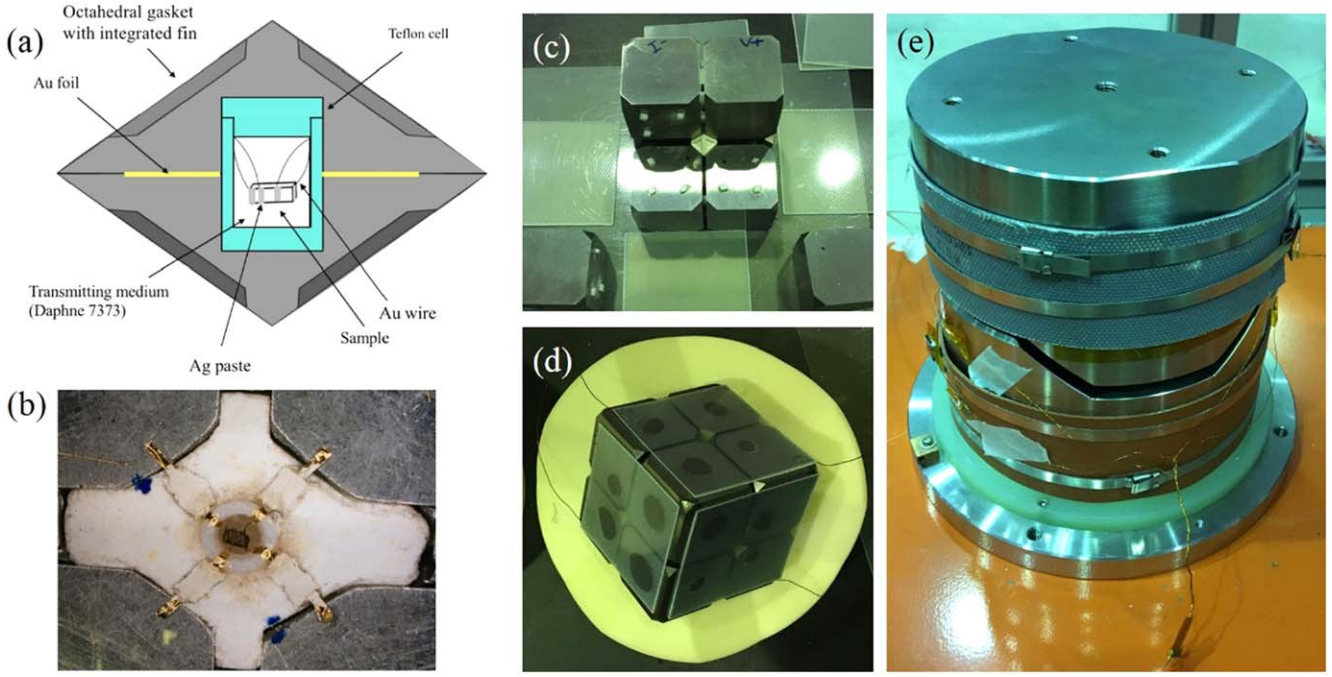

Figure 1. Experimental setup for high-pressure resistance measurements with a two-stage multianvil apparatus. (a) A cross-section view of the sample configuration for the resistance measurement with standard four-terminal method, (b) a photo of the sample installed in the Teflon capsule, (c) the octahedron surrounded by the second-stage tungsten carbide (WC) anvils, (d) the cluster of WC anvils held together with the insulating Fiber Reinforced Polymer (FRP) pads; (e) the pair of cylindrical first-stage anvils driving the WC anvils in the (111) direction.

Finally, the assembled second-stage WC anvils was put inside the cubic cavity of cylindrical first-stage driving blocks shown in Fig. 1e.

The whole MA8 module was put inside a top-loading high-pressure cryostat, for which a 1000-ton automatic hydraulic press was employed to maintain a constant loading force over the MA8 module during the cooling and heating processes between 300 and 2 K. The pressure values were estimated from the pressure-loading force calibration curve, which was per-determined at room temperature by detecting the characteristic phase transitions of Bi (2.55, 2.7, 7.7 GPa), Sn (9.4 GPa), Pb (13.4 GPa), ZnS (15.6 GPa) and GaAs (18.3 GPa) in electrical resistance. This is the common practice for pressure determination in the large-volume multianvil modules, and the accuracy of pressure is better than 1 GPa in the studied pressure range according to our experience. More detailed information about the low-temperature MA8 apparatus and the pressure calibrations can be found in our previous publication.[30]

Since the cooling of sample in the MA8 module is achieved by directly filling the cryostat with liquid nitrogen and then helium, it is difficult to control the cooling rate. In addition, the pushing columns driving on the MA8 module experience a strong contraction upon cooling down, which is compensated by the frequent movements of the hydraulic press in order to maintain a constant loading force on the MA8 module. These factors make the resistance data $R(T)$ during cooling down quite noisy and thus we always collect the $R(T)$ data upon warming up slowly by turning on the resistance heater surrounded on the first-stage anvils, Fig. 1e. After reaching near room temperature, we change pressure to the next target value while measuring $R(P)$ and then perform the thermal cycling again to measure $R(T)$ at constant pressure. It is noted that the resistance-type Cernox temperature sensor is placed in a hole of the first-stage anvil, Fig. 1e, and it is not under any pressure during the compression process.

Figure 2a shows the temperature-dependent resistance $R(T)$ of $LiOsO_3$ recorded upon warming up under different pressures from 5.0 to 18.5 GPa. Note that the $R(T)$ data in some temperature ranges at 5.0 and 12.7 GPa were missed due to the accidental disconnection of the temperature sensor. But this problem does not affect the determination of T_s at these two pressures and the main conclusion of this work. At ambient pressure, the non-polar to polar phase transition at T_s reflects as an anomaly in the temperature dependence of resistivity $\rho(T)$.[1] The anomaly in $\rho(T)$ has been used as an indicator to track down the change of T_s under high pressure.[13] However, the anomaly becomes significantly broad at $P > 5$ GPa as seen from the plot of dR/dT vs T in the previous study.[13] As shown in Fig. 2a, the nonpolar to polar transition at T_s in $LiOsO_3$ is still clearly visible as a slope change in $R(T)$ at 5 GPa as that at ambient pressure. The difference with the results from the previous study can be attributed to the hydrostaticity maintained to higher pressure in the MA8 apparatus. The transition temperature T_s can be precisely determined from derivative of resistivity, dR/dT, shown in Fig. 2b. Again, the anomaly in dR/dT vs T can be well defined at T_s up to 15.5 GPa, which is in sharp contrast to the broad humps at $P >$ 5 GPa in the previous study.[13] T_s is about 140 K at ambient pressure. At the first measured pressure of 5.0 GPa, T_s has been enhanced significantly to 204 ± 12 K, which is close to that reported by Aulestia et al.[13] As can be seen clearly, the transition at T_s is continuously shifted to higher temperatures progressively by pressure, and reaches about 285 ± 7 K at 15.5 GPa. This confirms that the polar phase has indeed been stabilized near room temperature, consistent with the high-pressure structure study.[14] For $P \leqslant 15.5$ GPa, the $R(T)$ behaves similarly except that the magnitude of resistance in the vicinity of T_s is reduced gradually accompanying the enhancement of T_s. But the resistance at low temperatures changes only slightly. In addition, the transition around T_s in $R(T)$ becomes broad in the pressure range 8–13 GPa. Even more significant broadening of the anomaly at T_s has also been encountered in the previous high-pressure transport study on $LiOsO_3$.[13] Such a broad transition under pressure should be caused by the pressure inhomogeneity or the presence of sheer stress.[14]

The behavior of $R(T)$ at 18.5 GPa is altered significantly in comparison with those at $P \leqslant 15.5$ GPa. A close inspection of dR/dT in Fig. 2b reveals a rather weak anomaly at $T_s = 285 \pm 9$ K, which indicated that the transition to polar phase still exists. As seen in Fig. 2a, in a wide temperature range below T_s, the $R(T)$ at 18.5 GPa exhibits a dominant concave curvature and shows a crossover to the

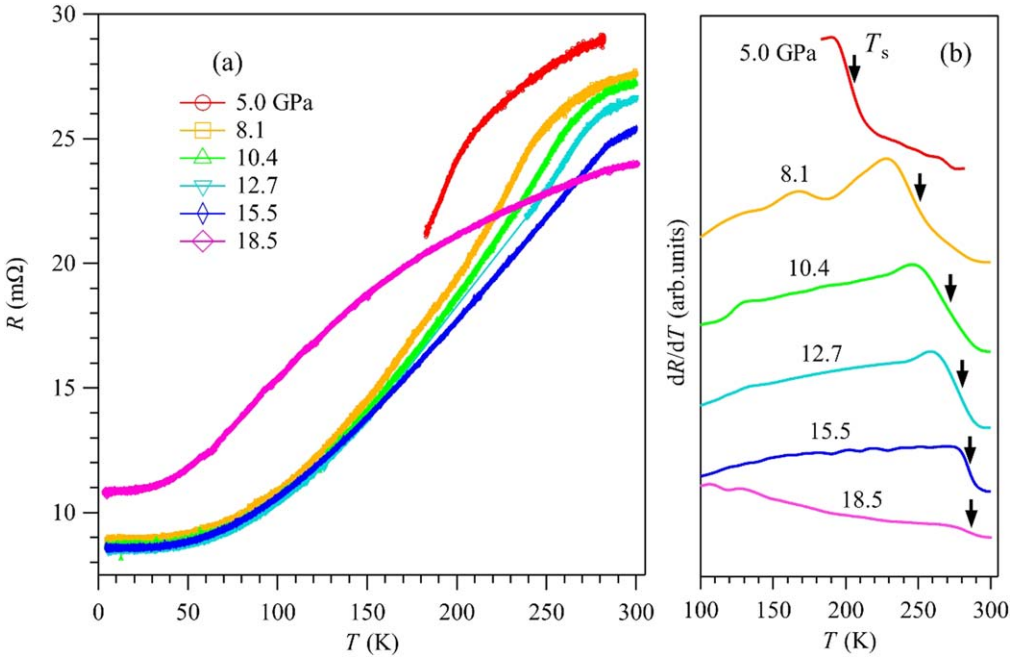

Figure 2. Temperature dependence of (a) resistance $R(T)$ and (b) its derivative dR/dT of $LiOsO_3$ crystal under various pressures up to 18.5 GPa recorded in the warming-up process. The transition temperatures T_s are marked by the arrows.

convex curvature only at temperatures below $\sim$ 80 K. This behavior is in strikingly different from that of the $R(T)$ curves at $P \leqslant$ 15.5 GPa, which are all featured by a convex curvature at $T < T_s$. Similar behaviors are commonly observed in the correlated metals without long-range magnetic order such as $CaRuO_3$[32] and $LiOsO_3$ at $T > T_s$. It is noteworthy that the residual resistivity at 18.5 GPa is enhanced significantly. According to the Matthiessen's rule, the residual resistivity of metals refers to the temperature-independent resistivity at temperatures approaching absolute zero where the electron scattering by lattice vibrations can be neglected and the electrons are mainly scattered by the impurities and defects in the metal. Since the impurity/defect concentration appears not to change with pressure, an abrupt increase of the residual resistivity indicates that there is a new phase of $LiOsO_3$ under 18.5 GPa where the electron's mobility is more sensitive to the impurity/defect.[33,34] The critical pressure for this transition is evidenced from pressure-dependent resistance $R(P)$ at room temperature shown below.

Figure 3 shows the $R(P)$ data in several segments recorded when changing pressures near room temperature. Note that some discontinuous jump of resistance between segments are caused by slightly different temperatures when the $R(P)$ measurements were performed. Basically, the resistance decreases smoothly with increasing pressure in each segment at $P \leqslant$15.5 GPa, whereas an obvious step-like anomaly is visible in $R(P)$ upon applying pressure from 15.5 to 18.5 GPa, signaling the occurrence of possible pressure-driven phase transition. The critical pressure of $P_c = 16.8(1)$ GPa can be determined from the sharp dip of dR/dP shown in Fig. 3.

As mentioned above, Aulestia et al.[13] revealed a linear increase of $T_s(P)$ with a large slope of $dT_s/dP \approx +17.54$ K GPa^{-1} by monitoring the anomaly in resistance up to 6.48 GPa. If this trend is kept, one would expect T_s to reach 295 K at $\sim$ 9.5 GPa. However, high-pressure Raman and SXRD experiments support that the polar structure is stabilized at room temperature at 12.6–15.5 GPa.[14] Complementary to these previous studies, the present work resolves the above discrepancy by mapping out the complete pressure evolution of $T_s(P)$ as shown in Fig. 4. The $T_s(P)$ determined by Aulestia et al.[13] is also plotted in Fig. 4 for comparison. As can be seen clearly, $T_s(P)$ first increases almost linearly with pressure at a large slope and then levels off at pressures above 10 GPa. According

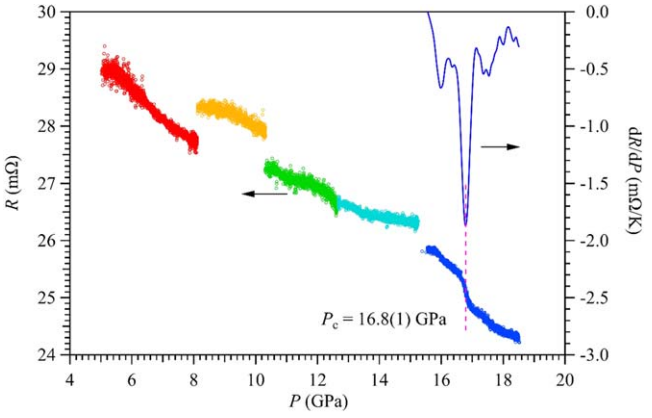

Figure 3. Pressure-dependent resistance $R(P)$ in several segments recorded when changing pressures near room temperature. The discontinuous jump of resistance between some segments is caused by the temperature difference. When applying pressure from 15.5 to 18.5 GPa, an obvious step-like anomaly is observed at about $P_c = 16.8(1)$ GPa as indicated by the sharp dip of dR/dP.

to the SXRD results, the phase below T_s in the investigated pressure range should adopt the *R3c* polar structure. As such, the observed $R(P)$ anomaly at $P_c \approx 16.8$ GPa and the distinct $R(T)$ behaviors at $P =$ 18.5 GPa $> P_c$ should be attributed to a novel electronic state in the polar metal $LiOsO_3$. Whether this new electronic state is associated with some local structural distortions deserves further investigations.

These new resistance data obtained in a wide pressure range by employing the MA8 apparatus allowed us to construct a more comprehensive $T_s(P)$ phase diagram of $LiOsO_3$ and to uncover a possible novel electronic state above 16.8 GPa in the polar phase. As seen in Fig. 4, the deviation of $T_s(P)$ from the linear behavior and the smooth crossover to the saturation behavior suggest the presence of two competing factors influencing the polar phase. On the one hand, pressure favors the polar *R3c* phase with a smaller volume, leading to a quick rise of $T_s(P)$. According to the density-functional-theory (DFT) calculations,[13] the polar distortions of *R3c* phase is strengthened by pressure. On the other hand, the calculations also found that

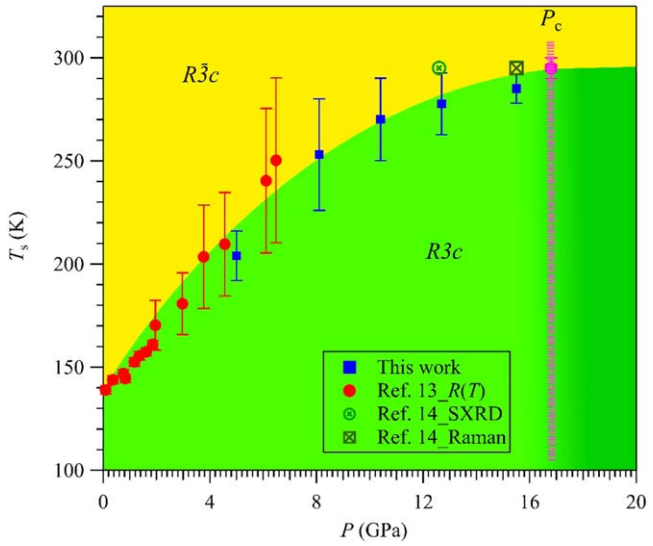

Figure 4. Temperature-pressure phase diagram of $LiOsO_3$.

the centrosymmetric *Pbnm* structure becomes more stable than the nonpolar $R\bar{3}c$ phase above 8 GPa and even more stable than the polar *R3c* phase above 21 GPa. The polar *R3c* phase is retained up to at least 42 GPa, but the reliability factors of the structural refinement go higher at $P > 20$ GPa based on the SXRD results,[14] which may make the validity of using the *R3c* model questionable for the phase at $P > 20$ GPa. The tendency to stabilize the *Pbnm* structure under higher pressure would compete and thwarted the enhancement of T_s.

In conclusion, we have tracked the nonpolar to polar transition of $LiOsO_3$ crystal to near room temperature by measuring the $R(T)$ in a MA8 apparatus up to 18.5 GPa. Whereas the polar phase in $LiOsO_3$ can be stabilized near room temperature under 18.5 GPa, there is a pressure-driven electronic phase transition at $P \approx 17$ GPa, which has not been detected by the in situ structural and Raman studies under high pressure.

Acknowledgments

JGC thank Shan Yu, Kento Ishigaki, Jun Gouchi, and Shoko Nagasaki for the assistance on high-pressure experiments with the MA8 apparatus during his stay in ISSP, University of Tokyo as a visiting professor. JGC also thanks Yanfeng Guo for providing a $LiOsO_3$ crystal for initial high-pressure measurements, Ziyi Liu and Keyu Chen for analyzing the resistance data and making the color plot of Fig. 4. This work was partially supported by National Key R&D Program of China (2018YFA0305700), the National Natural Science Foundation of China (12025408, 11874400, 11834016, 11921004), the Beijing Natural Science Foundation (Z190008). JSZ was supported by NSF grants DMR 1905598 and MRSEC DMR1720595 in USA. YU acknowledges the support from JSPS KAKENHI (19H00648).

ORCID

J.-G. Cheng https://orcid.org/0000-0002-4969-1960

References

1. Y. Shi et al., *Nature Mater.*, **12**, 1024 (2013).
2. G. Giovannetti and M. Capone, *Phys. Rev. B*, **90**, 195113 (2014).
3. Q. Yao, H. Wu, K. Deng, and E. Kan, *RSC Adv.*, **4**, 26843 (2014).
4. H. M. Liu, Y. P. Du, Y. L. Xie, J.-M. Liu, C.-G. Duan, and X. Wan, *Phys. Rev. B*, **91**, 064104 (2015).
5. P. Li, X. Ren, G.-C. Guo, and L. He, *Sci. Rep.*, **6**, 34085 (2016).
6. Y. Zhang, J. Gong, C. Li, L. Lin, Z. Yan, S. Dong, and J.-M. Liu, *Phys. Status Solidi RRL*, **12**, 1800396 (2018).
7. H. Sim and B. G. Kim, *Phys. Rev. B*, **89**, 201107(R) (2014).
8. H. J. Xiang, *Phys. Rev. B*, **90**, 094108 (2014).
9. C. He, Z. Ma, B.-Z. Sun, Q. Li, and K. Wu, *Comput. Mater. Sci.*, **105**, 11 (2015).
10. Y. Zhang, J. Gong, C. Li, L. Lin, Z. Yan, S. Dong, and J.-M. Liu, *Phys. Status Solidi RRL*, **13**, 1900436 (2019).
11. F. Jin, A. Zhang, J. Ji, K. Liu, L. Wang, Y. Shi, Y. Tian, X. Ma, and Q. Zhang, *Phys. Rev. B*, **93**, 064303 (2016).
12. H. Padmanabhan, Y. Park, D. Puggioni, Y. Yuan, Y. Cao, L. Gasparov, Y. Shi, J. Chakhalian, J. M. Rondinelli, and V. Gopalan, *Appl. Phys. Lett.*, **113**, 122906 (2018).
13. E. I. Paredes Aulestia, Y. W. Cheung, Y.-W. Fang, J. He, K. Yamaura, K. L. Lai, S. K. Goh, and H. Chen, *Appl. Phys. Lett.*, **113**, 012902 (2018).
14. J.-J. Gao, S.-Y. Fu, K. Yamaura, J. F. Lin, and J.-S. Zhou, *Phys. Rev. B*, **101**, 220101(R) (2020).
15. J.-S. Zhou, X. Li, J. M. He, J. Chen, and K. Yamaura, *Phys. Rev. B*, **104**, 115130 (2021).
16. I. Lo Vecchio, G. Giovannetti, M. Autore, P. Di Pietro, A. Perucchi, J. He, K. Yamaura, M. Capone, and S. Lupi, *Phys. Rev. B*, **93**, 161113(R) (2016).
17. N. J. Laurita, A. Ron, J.-Y. Shan, D. Puggioni, N. Z. Koocher, K. Yamaura, Y. Shi, J. M. Rondinelli, and D. Hsieh, *Nature Commun.*, **10**, 3217 (2019).
18. E. Berger et al., *Nano Lett.*, **21**, 6095 (2021).
19. Y. R. Wang, S. Wang, H. L. Tao, Y. Cui, S. M. Liu, M. He, B. Song, and Z. H. Zhang, *Solid State Commun.*, **323**, 114099 (2021).
20. D. Puggioni, G. Giovannetti, M. Capone, and J. M. Rondinelli, *Phys. Rev. Lett.*, **115**, 087202 (2015).
21. J. Lu, G. Chen, W. Luo, J. Iniguez, L. Bellaiche, and H. Xiang, *Phys. Rev. Lett.*, **122**, 227601 (2019).
22. N. A. Benedek and T. Birol, *J. Mater. Chem. C*, **4**, 4000 (2016).
23. C. Ma and K. Jin, *Sci. China-Phys. Mech. & Astron.*, **61**, 097011 (2018).
24. W. X. Zhou and A. Ariando, *Jpn. J. Appl. Phys.*, **59**, SI0802 (2020).
25. A. Zabalo and M. Stengel, *Phys. Rev. Lett.*, **126**, 127601 (2021).
26. A. Narayan, *J. Phys. Condens. Matter*, **32**, 125501 (2020).
27. G. A. Samara, T. Sakudo, and K. Yoshimitsu, *Phys. Rev. Lett.*, **35**, 1767 (1975).
28. I. A. Kornev and L. Bellaihe, *Phase Transit.*, **80**, 385 (2007).
29. T. Ishidate, S. Abe, H. Takahashi, and N. Mori, *Phys. Rev. Lett.*, **78**, 2397 (1997).
30. K. Ishigaki, J. Gouchi, S. Nagasaki, J.-G. Cheng, and Y. Uwatoko, *Papers in Physics*, **11**, 110006 (2019).
31. K. Yamaura, *J. Solid State Chem.*, **236**, 45 (2016).
32. L. Klein, L. Antognazza, T. H. Geballe, M. R. Beasley, and A. Kapitulnik, *Physica B*, **259-261**, 431 (1999).
33. D. Errandonea, A. Segura, D. Martinez-Garcia, and V. Munoz-San Jose, *Phys. Rev. B*, **79**, 125203 (2009).
34. H. Saqib, S. Rahman, Y. Zhao, C. Cazorla, D. Errandonea, R. Susilo, Y. Zhuang, Y. Huang, B. Chen, and N. Dai, *J. Phys. Chem. Lett.*, **12**, 9859 (2021).